Suitability of a constant air temperature lapse rate over an Alpine glacier: testing the Greuell and Böhm model as an alternative

Lene PETERSEN,[1] Francesca PELLICCIOTTI,[1] Inge JUSZAK,[1] Marco CARENZO,[1] Ben BROCK,[2]

[1]*Institute of Environmental Engineering, ETH Zurich, Zurich, Switzerland*

E-mail: petersen@ifu.baug.ethz.ch

[2]*School of the Built and Natural Environment, Northumbria University, Newcastle Upon Tyne NE1 8ST, UK*

ABSTRACT. Near surface air temperature, typically measured at a height of 2 m, is the most important control on the melt rate at a snow or ice surface. It is distributed in an overly-simplistic manner in most glacier melt models by using constant linear lapse rates, which poorly represent the actual spatial and temporal variability of air temperature. In this study we test a simple thermodynamic model proposed by Greuell and Böhm in 1998 as an alternative, using a new data set of air temperature measurements from along the flowline of Haut Glacier d'Arolla, Switzerland. The unmodified model performs little better than assuming a constant linear lapse rate. When modified to allow the ratio of the boundary layer height to the bulk heat transfer coefficient to vary along the flowline, the model matches measured air temperatures better and a further reduction of the Root Mean Square Error is obtained, although there is still considerable scope for improvement. The modified model is shown to perform best under conditions favourable to the development of katabatic winds: few clouds, positive ambient air temperature, limited influence of synoptic or valley winds and a long fetch, but its performance is poor under cloudy conditions.

1. INTRODUCTION

Near surface temperature, T_a, typically measured at a height of 2 m, is the most important control on the energy exchange and melt rate at a snow or ice surface. For spatially distributed glacier melt modelling a distributed temperature input is needed, which is normally generated by extrapolation from point measurements with a linear lapse rate (LR). The LR describes the dependency of temperature with elevation and is considered to be positive when temperature increases with elevation (e.g. Minder and others, 2010). A steep (strongly negative) LR indicates a fast decrease of temperature with increasing altitude (see e.g. Pepin and Losleben, 2002). In most glacier melt models, the temperature is represented with a constant in time and uniform in space LR (e.g. Klok and Oerlemans, 2002; Hock and Holmgren, 2005; Machguth and others, 2006; Huss and others, 2008; Farinotti and others, 2012). Generally such a LR lies between -0.0055 and -0.0065 °C/m (e.g. Arnold and others, 2006; Machguth and others, 2006; Michlmayr and others, 2008; Gardner and Sharp, 2009; Paul and others, 2009; Nolin and others, 2010), the latter often being referred to as the Environmental Lapse Rate (ELR) (or mean Moist Adiabatic Lapse Rate (MALR)). Both the assumption of a constant in time and uniform in space LR, and the use of the ELR have been recently questioned for high elevation and glacierised basins. Most studies on the variability of near-surface temperature LRs over glaciers have found generally lower LRs than the ones commonly used (e.g. Strasser and others, 2004; Li and Williams, 2008; Hulth and others, 2010), while Minder and others (2010) pointed out that there is no physical basis for the use of the ELR in high elevation basins where the effect of the terrain cannot be neglected. Spatio-temporal patterns of air temperature variability have been shown to be affected by various factors of the surface environment and atmospheric conditions (see Marshall and others, 2007), so that the application of free atmosphere LRs is questionable. Temporal variability has been shown to be important at all scales in various studies (e.g. Stahl and others, 2006; Marshall and others, 2007; Gardner and others, 2009; Chutko and Lamoureux, 2009; Petersen and Pellicciotti, 2011), while spatial variations are more complex than the simple linear dependency with elevation assumes (e.g. Strasser and others, 2004; Brock and others, 2010; Petersen and Pellicciotti, 2011). An additional limitation of to the use of a constant LR to extrapolate air temperature from off-glacier stations is that changes in temperature off-glaciers are in general higher than on-glacier because of the dampening effect of the glacier (Greuell and Böhm, 1998). This effect cannot be taken into account by use of a simple LR and the higher temperature changes would be translated as such onto the glacier surface.

Lack of extensive T_a data sets on glaciers is a key restriction for a thorough analysis of temperature variability in space and time, as well as for development of models. Using a high resolution data set of temperature time series at several locations along the glacier flowline of Juncal Norte Glacier, Chile, Petersen and Pellicciotti (2011) found a strong diurnal LR cycle driven by the development of a katabatic boundary layer (KBL), with steeper LRs in the afternoon when katabatic wind was eroded and elevation was reestablished as the main control of air temperature variability. A KBL develops on melting glaciers

when the air temperature above the glacier, which is normally higher than that of the glacier surface (which cannot exceed 0°C), is cooled by the surface. The cooling increases its density and the resulting density gradient produces katabatic flow (e.g. Ohata, 1989; Greuell and others, 1997; Klok and others, 2005; Pellicciotti and others, 2008). Most studies using procedures to generate temperature fields to drive melt models do not account for processes within the KBL (Shea and Moore, 2010) even though it is a main control over temperature variability. The presence of the KBL affects the thermal regime by reinforcing the turbulent exchange of heat by sensible fluxes and the cooling of the air adjacent to the surface. As a result, temperatures within the KBL are cooler than those outside (Greuell and Böhm, 1998; Marshall and others, 2007; Shea and Moore, 2010). Empirical approaches to take into account the difference in regime between on and off-glacier temperature have been suggested by Shea and Moore (2010) and Braithwaite and others (2002). An attempt to include these effects was proposed by Greuell and Böhm (1998) with a thermodynamic model (henceforth referred to as GB98) in which air temperature is derived as a function of slope and distance along the flowline. This approach was suggested as variations in air temperature along the valley glacier Pasterze Glacier, Austria, could not be explained by means of a constant LR (see section 4). GB98 is, to our knowledge, the only model of air temperature distribution on glaciers that has been suggested as a realistic and practical alternative to extrapolation using LRs. However, there has been little published work applying the model to other glaciers or testing its main assumptions. The aim of this paper is therefore to investigate the suitability of the GB98 model for calculation of air temperature distribution across a well studied alpine glacier, Haut Glacier d'Arolla (HGdA, see Figure 1), in the Swiss Alps, and to explore its strengths and limitations in comparison with the commonly used LR approach. For this, we make use of a new data set of distributed temperature records collected on HGdA during the 2010 ablation season.

2. EXPERIMENTAL SETUP

Our study site is HGdA, in the Val d'Hérens in southern Switzerland (Figure 1a). It has an area of 4 km^2 and a length of 4 km and comprises two basins feeding a tongue. The elevation ranges from 2590 m to about 3500 m with a generally constant and gentle slope (see Figure 1b). About 36 % of the basin is glacierised. Numerous studies of glacier energy balance and ablation, meteorology and hydrology have been conducted on the glacier (e.g. Nienow and others, 1996; Arnold and others, 1996; Willis and others, 2002; Pellicciotti and others, 2005; Brock and others, 2006; Carenzo and others, 2009).

In 2010, a glacio-meteorological field campaign was conducted from 24th of May until the 12th of September. The setup included 5 Automatic Weather Stations (AWSs) and 7 T-Loggers used in this study (see Figure 1a). The AWSs measured at a 5-second interval and stored averaged 5-minute records of air temperature (°C), relative humidity (%), wind speed (ms^{-1}), wind direction (°), and incoming and reflected shortwave radiation (Wm^{-2}). The thermometers of AWS2, AWS3 and AWS4 were ventilated and shielded, while AWS1 and AWS5 were shielded but not ventilated. The T-Loggers consisted of a HOBO TidbiT v2 UTBI-001 temperature sensor with integrated datalogger housed in a shielded PVC cylinder and fixed to a metal

tripod 2 m above the surface. The details of this setup are described in Petersen and Pellicciotti (2011). The T-Loggers used in this study were located along the glacier flowline, some of them close to the AWSs (Figure 1a). They measured at an interval of 5 or 10 minutes. All data were aggregated to hourly values for the analysis. The characteristics of the AWSs and T-Loggers are listed in Table 1. In this work, we mainly use the temperature data from the T-Loggers for the analysis of the temporal and spatial variability of 2 m air temperature and testing of the model, and the data from the AWSs for analysis of wind direction and derivation of cloud transmittance factors. We also use data measured at two permanent off-glacier stations, AWS-T1 and AWS-T2 (Figure 1a). AWS-T1 is located on rock near the glacier terminus at an elevation of 2500 m. AWS-T2 is set up on periglacial debris of the easterly slopes next to the glacier at an elevation of 2990 m. Longwave radiation (Wm^{-2}) and temperature ($^{\circ}$C) from the two off-glacier AWSs are used for the calculation of cloud cover and the corresponding classification in cloud classes (Section 5). The temperature record of AWS-T2 provides the input to the model. Some of the T-Loggers fell down on the glacier surface during certain periods which were therefore excluded. For the analysis we use only the data when all T-Loggers were functioning, so that the data set consists of 1284 hours of non-continuous measurements. TL6 was not considered in the analysis due to a very short functioning period. This common period (indicated by the grey bar in Figure 4) is used to compute the main statistics for the temperature series at each T-Logger (Table 1). An airborne LiDAR (Light Detection And Ranging) flight over the HGdA glacier basin in October 2010 by Helimap System SA provided a DEM (Digital Elevation Model) with a grid resolution of 10 m, which is used as the basis of the model in this paper, in particular to derive the glacier slope and the distance along the flowline (see Figure 1 for details). The elevations of the AWSs and T-Loggers were measured with differential GPS.

3. APPLICATION OF A CONSTANT LAPSE RATE (CLR)

We calculated a constant in time and uniform in space LR using the data from the T-Loggers, as well as a LR variable in time, to test the validity of the commonly used method of T_a extrapolation on HGdA. The data show high temporal variability on different scales as well as spatial variations across the glacier (Figure 2a). The figure shows the lapse rate calculated through linear regression using i) all T-Loggers, ii) all T-Loggers in the lower part of the glacier (TL7, TL8, TL9) and iii) all T-Loggers in the upper part (TL1, TL2, TL3). The differences at both spatial and temporal scale are significant. The lower section of the glacier is characterized by steep, negative LRs while the upper section has less negative LRs or even positive ones, indicating inversions. Use of one single variable LR for the entire glacier averages out the two behaviors, also reducing the observed temporal variability. If the LR is also averaged in time over the season, we obtain an unrealistic value that only results from compensation of contrasting patterns. It is thus evident that application of a constant LR would not represent the actual temperature variability over the glacier, in time nor space. Figure 2b shows the comparison of observed temperature with temperature extrapolated from AWS-T2 with the ELR (-0.0065 $^{\circ}\mathrm{Cm}^{-1}$) and a calibrated constant LR (CLRcal). Previous

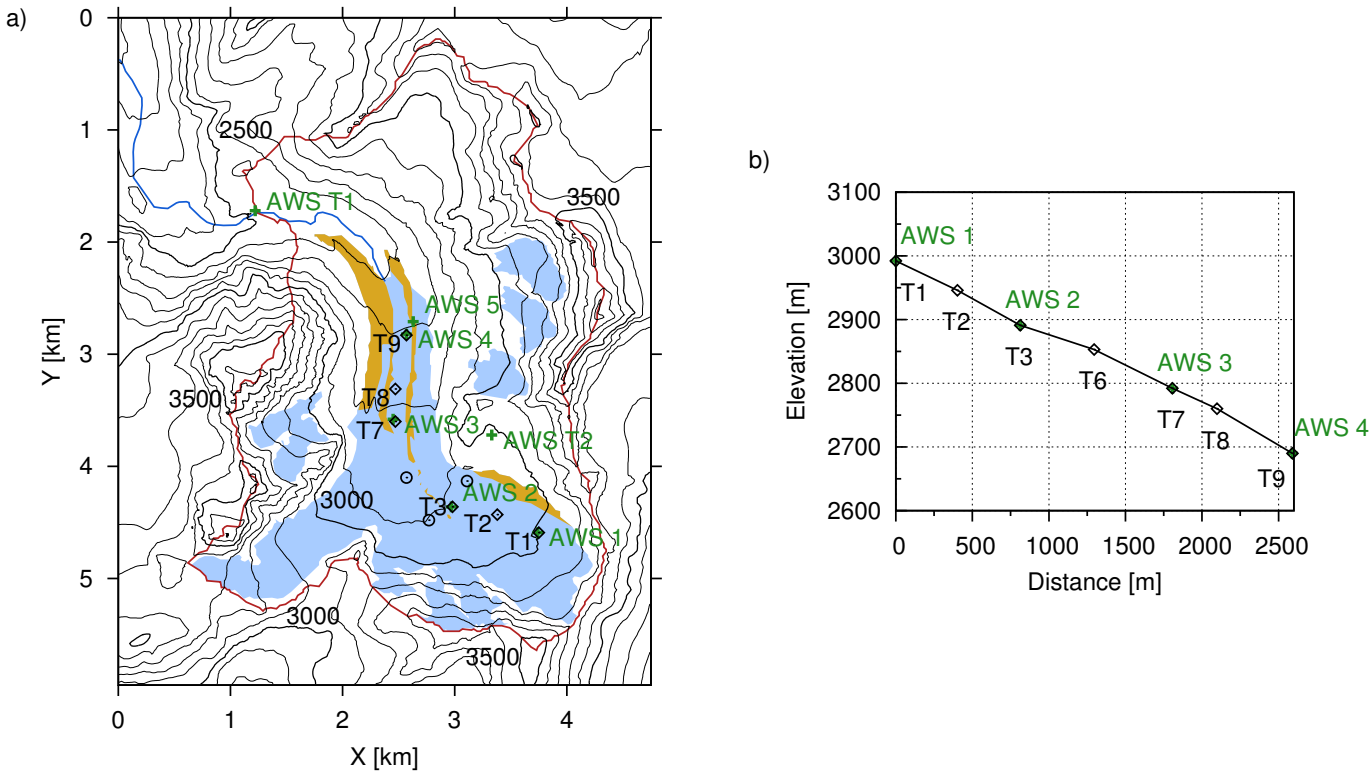

Fig. 1. a) Map of Haut Glacier d'Arolla showing the glacierised area (blue), the debris covered area (brown) and the catchment outline (red). Green '+' indicates the locations of AWS in 2010, 'o' indicates the positions of T-loggers which are not used in the analysis; the T-loggers along the flowline are indicated with diamonds and labeled. The upper left corner of the plot is 604030, 94910 in Swiss coordinates. b) Surface profile along the flowline. AWS5 is approximately at the same elevation as AWS4.

to the extrapolation, data at AWS-T2 were corrected. A systematic difference between the temperature data at AWS-T2 and at the uppermost T-Logger TL1 is evident (Table 2). Although the two stations are at almost the same elevation, the mean temperature over the common period is about 0.5 °C colder at AWS-T2 than at the location on the glacier (Table 2). This effect might be due to the location of AWS-T2 being windier and to the air being better mixed. It could also be caused by differences in the ventilation of the sensors as well as by the fact that the boundary layer at TL1 might be thin and thus the station might measure outside of the GBL. However, the exact cause cannot be identified precisely given the limited amount of data available. To exclude this systematic error, we corrected the temperature at AWS-T2 with an offset of 0.5 °C. The constant LR was calibrated by minimizing the Root Mean Square Error (RMSE) at all T-Logger locations over the whole time series for the common period of record. The CLRcal is equal to -0.0032 $^{\circ}\mathrm{Cm}^{-1}$ and thus shallower than the ELR, confirming evidence from previous studies (e.g. Marshall and Sharp, 2008; Shea and Moore, 2010). Use of an ad hoc calibrated LR provides an obvious improvement over the use of the standard ELR (Figure 2b).

Table 1. Characteristics of the AWSs and T-Loggers: name, elevation, X-Coordinate, Y-Coordinate, mean temperature and standard deviation (std). Mean temperature and standard deviation are calculated over the common period of record (1284 hours) unless stated otherwise. The elevation and coordinates of the AWSs and T-Loggers were measured with a differential GPS. *over bare ground. **not ventilated. ***only measuring the first weeks during a relatively cold period.

Name	Elevation (m)	X-Coordinate (m)	Y-Coordinate (m)	Mean Temp. (°C)	Std Temp (°C)
AWS-T1*	2500	605248	93193	5.86	4.28
AWS-T2*	2990	607356	91193	2.87	4.21
AWS1**	2992	607766	90330	3.10	4.00
AWS2***	2890	606987	90560	1.21	3.19
AWS3	2797	606489	91326	3.04	3.27
AWS4	2680	606588	92097	5.04	4.17
AWS5**	2662	606655	92207	4.61	3.84
TL1	2992	607766	90330	3.36	3.94
TL2	2946	607407	90482	3.53	3.82
TL3	2891	606987	90560	3.44	3.61
TL6***	2853	606594	90814	(2.11)	(3.52)
TL7	2792	606489	91326	3.75	3.38
TL8	2760	606576	91609	4.00	3.43
TL9	2680	606588	92050	4.75	3.78

4. APPLICATION OF THE GREUELL AND BÖHM MODEL (GB98)

In the description of the GB98 model we follow the naming convention of the original paper. The main assumption of this simple thermodynamic model is that temperature distribution over a melting glacier is a balance between adiabatic warming (cooling) due to compression (expansion) of air moving along the glacier and the sensible heat exchange with the underlying ice surface (see van den Broeke, 1997). Hence, air temperature distribution is parameterized as mainly a function of slope and along-glacier distance. Temperature changes due to surrounding topography, entrainment, phase changes, radiation divergence and variation of fluxes in the horizontal direction are neglected. These assumptions were based on results obtained by van den Broeke (1997) on Pasterze glacier during the 1994 summer season. The author argued from analysis of wind directions that conditions on Pasterze were mostly dominated by the katabatic or glacier wind. The model is based on a number of other simplifying assumptions, such as that the height of the glacier wind layer (H) and the glacier slope are constant. These

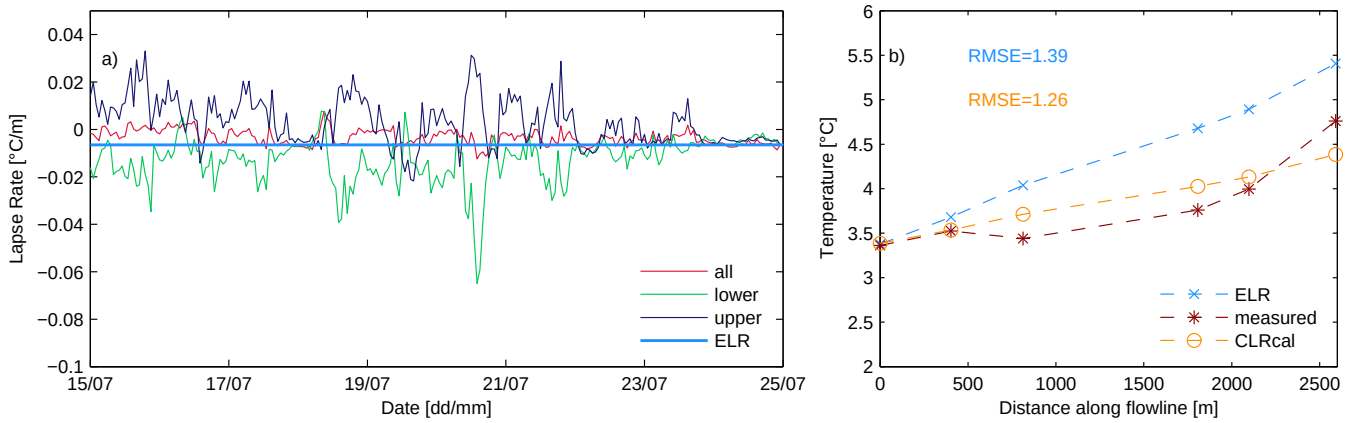

Fig. 2. a) Comparison of the constant ELR with LRs variable in space and time: regression of all T-Loggers along the flowline (TL1,TL2,TL3,TL7,TL8,TL9) (indicated with "all"); upper LR (indicated by "upper") obtained from regression of the upper T-Loggers (TL1,TL2 and TL3) and lower LR (indicated by "lower") obtained from regression of the lower T-Loggers (TL7, TL8 and TL9). b) Comparison of mean observed temperature at each T-Logger with temperature extrapolated from AWS-T2 with the ELR and the calibrated constant LR (CLRcal). Also indicated is the Root Mean Square Error (RMSE) for the two model versions.

assumptions were discussed by Greuell and Böhm (1998) for the Pasterze Glacier and will be addressed in the following section. Since the model is based on the hypothesis that the glacier wind is present, a requirement for its application is an air temperature greater than the surface temperature so that the glacier wind is likely to develop (see Section 1).

For the application of the model, the glacier geometry must be known in order to derive slope angle and distance along the glacier flowline. This information can be extracted from glacier DEMs that can also be provided by downloadable global databases, e.g. glacier outlines from the World Glacier Monitoring Service/Global Land Ice Measurements from Space (WGMS/GLIMS) and DEMs from the Shuttle Radar Topography Mission (SRTM), which makes the model appealing in terms of applicability. We used the DEM described in Section 2 above. Here we report only the main equations of the model and refer the reader to the original paper by Greuell and Böhm (1998) for more details. The potential temperature Θ is calculated as

$$\Theta(x) = (T_0 - T_{eq}) \exp(-\frac{x - x_0}{L_R}) - b\,(x + x_0) + T_{eq} \tag{1}$$

From this, the actual temperature can be derived as:

$$T(x) = (T_0 - T_{eq}) \exp(-\frac{x - x_0}{L_R}) + T_{eq} \tag{2}$$

with:

$$T_0 = T_{cs} - \gamma\,(z_{cs} - z_0) \tag{3}$$

$$T_{eq} = b\,L_R \tag{4}$$

$$b = \Gamma\,tan(\alpha) \tag{5}$$

$$L_R = \frac{H\,cos(\alpha)}{c_H} \tag{6}$$

where $T(x)$ is the temperature at a distance x along the glacier flowline, T_0 the temperature at x=0, T_{eq} the equilibrium temperature value, Γ the dry adiabatic LR (-0.0098 $^{\circ}$Cm^{-1}), c_H the bulk transfer coefficient for heat (see Stull (1988)) and T_{cs} and z_{cs} are the temperature and elevation of the climate station outside of the glacier's influence used to drive the model (AWS-T2 in our study). All equations above are based on the assumptions that the glacier slope is constant and that the ratio H/c_H is constant along the flowline.

The equations above contain five unknown parameters: x_0 and z_0, the location and elevation where the air parcel enters the layer influenced by the glacier, the length scale L_R and b (which are defined above and depend on the glacier slope (α)) and γ, the lapse rate used to extrapolate temperature from the input climate station (T_{cs}) to the initial point (x_0, z_0). Here we apply the model to the entire data set of temperature observations (common period of record), following the same approach as Greuell and Böhm (1998). We use the same values of γ (-0.007 $^{\circ}$Cm^{-1}), H (equal to 17 m as estimated for Pasterze by Greuell and Böhm (1998)) and c_H (0.002 following Stull (1988)) as used by the authors. We refer to this setup as the unmodified model, but test different assumptions for the position and elevation of the uppermost point of the flowline (x_0 and z_0), as recommended by GB98, who pointed to the fact that both x_0 and z_0 could be regarded as tuning parameters. The best fit is obtained by assuming the uppermost T-Logger (TL1) as the initial point (of coordinate x_0 and elevation z_0, respectively). Model sensitivity was then analysed by varying the other parameters by ± 10, 25 and 50 % around the initial values taken from Greuell and Böhm (1998). Variations in H (constant along the flowline), the slope (and thus b and L_R) and γ in the range above resulted in small changes in the temperature profile (not shown here). Varying γ (±10, 25 and 50%) did not have a major effect as expected considering the similar elevation of the climate station and of the initial point (TL1) (see Table 1). We also tested the effect of using different off-glacier data as input to the model, but the differences when using the nearest MeteoSwiss station Grand St. Bernard (2472 m, 579137/79856 m, located at a distance of 30.4 km) were negligible.

Figure 3a shows the comparison of measured air temperature with air temperature extrapolated with the calibrated constant LR (CLRcal) and modelled with the GB98 model, for the common period of record. Even though the CLRcal seems to work in an acceptable manner, the RMSE is reduced by 7% by applying the GB98. The CLRcal leads to underestimation of

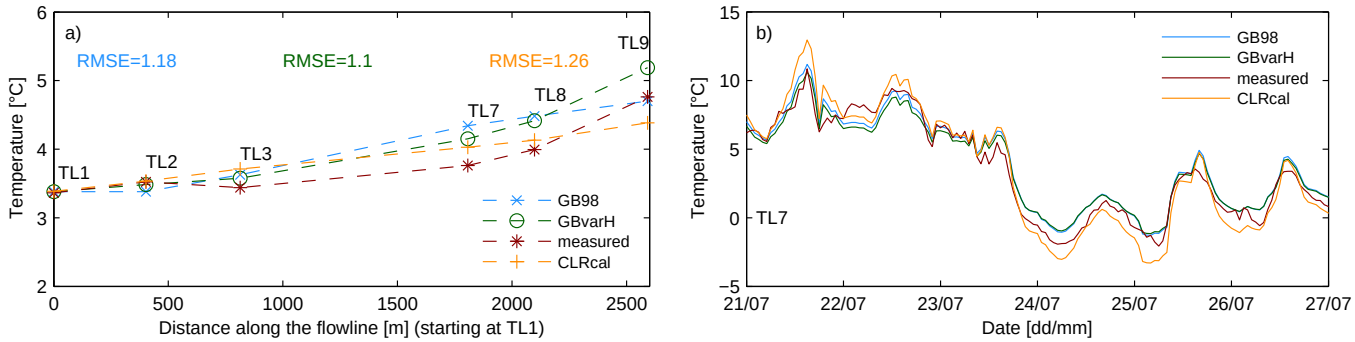

Fig. 3. Comparison of observed temperature and temperature modelled with the GB98 with the values of H, γ and Γ suggested in the original paper for Pasterze glacier (GB98, referred to in the text as unmodified model) and the modified version (GBvarH, Section 5): a) average values along the flowline; and b) time series at TL7 for a selected sub-period (21 to 27 of July).

temperatures during cold periods and overestimation during warm periods (Figure 3b). As these two errors compensate each other, the net effect is an apparent good performance if we look only at the average values over the season (Figure 3a).

The GB98 on average overestimates temperature in the central part of the glacier (TL3, TL7 and TL8). The observations reveal a profile along the glacier flowline that is characterised by average temperatures decreasing more slowly in the central part of the glacier than in the uppermost and lower sections (Figure 3b). This profile cannot be reproduced by the model, which exhibits a more linear change in air temperature with distance along the flowline than is observed.

5. APPLICABILITY OF THE GB98 MODEL UNDER DIFFERENT METEOROLOGICAL CONDITIONS

The results of the application of the GB98 model to the entire data set reveal that the model cannot reproduce the observed variability on HGdA in its original form (Figure 3), even if parameters are varied to adjust the model outputs to the observations.

The model is based on the assumption of two main fluxes controlling the exchange of energy at the glacier surface and affecting the temperature of air in the GBL (see Section 4), and it requires, in particular, that the glacier wind is well developed. The latter is generated by the temperature deficit between the glacier surface and overlaying air, which causes the air particles above the surface to cool down and gravitationally flow because of the associated increase in density (e.g. Stenning and others, 1981; Greuell and Böhm, 1998; van den Broeke, 1997). We therefore analysed the climatic conditions typical of the 2010 season in detail, to assess under which conditions the assumptions of the model are justified. We defined categories for air temperature, cloudiness and wind direction on a *daily* basis as follows:

1. *Temperature*: the temperature record was divided in two classes representative of cold and warm air temperature: i) T1, days for which more than 80% of the hourly values are above 0°C; and ii) T2, including the remaining cases. Most days fell into category T1, indicating the existence of conditions favouring the development of katabatic wind.

2. *Wind*: the influence of wind was investigated by defining four classes: i) W1, characterised by mainly downvalley wind (more than 80% of the hourly values); ii) W2, characterised by a diurnal cycle with mainly downvalley wind at night and in the morning hours (more than 60% of the hourly values between 21.00 and 12.00) and mainly upvalley wind in the afternoon hours (more than 60% of the hourly values between 13.00 and 20.00), which was identified as typical pattern of several days and a clear distinction from other conditions could be made; iii) W3, with a mixed wind pattern (all remaining cases); and iv) W4, with mainly upvalley wind (more than 80% of the hourly values). For this classification, we used the frequency distribution of the wind direction data from AWS4. However, the classification was compared to that obtained from the records at the other AWSs showing a nearly perfect correspondence.

3. *Cloud cover*: the categories for clouds were derived by classifying the days on the basis of cloud transmittance factors or cloud cover, n, derived from the measured incoming longwave radiation data at three AWSs (AWS-T1, AWS-T2 and AWS5). We adopted the approach by Marty and Philipona (2000), which is based on the comparison of the atmospheric emissivity eps_a and the potential clear-sky atmospheric emissivity eps_p (calculated with Brutsaert formula (Brutsaert, 1975), for the reasons explained in Marty and Philipona (2000)). The ratio of the two emissivities provides a clear-sky index, the complement of which is the cloud factor. This method was found to be superior to methods based on the ratio of potential clear-sky to measured shortwave radiation (which are often used (Brock and Arnold, 2000)), by Juszak and Pellicciotti (2012). The cloud cover was estimated on the basis of a linear regression between eps_p and 1, where $eps_a = eps_p$ corresponds to a cloud cover of zero and $eps_a = 1$ to a cloud-cover of one.

$$eps_a = \frac{lw}{\sigma T^4} \tag{7}$$

with T (K) being the air temperature, lw (Wm^{-2}) the measured incoming longwave radiation and σ the Stefan-Boltzmann constant. The daily cloud cover n was calculated as the mean of the hourly values at the three AWSs This value was then used to identify 4 categories: i) C1: $n > 0.8$ overcast days ; ii) C2: $0.4 < n \leq 0.8$ days with considerable cloud cover ; iii) C3: $0.1 < n \leq 0.4$ days with few clouds; and iv) C4: $n \leq 0.1$ clear-sky days.

The categories are listed in Table 2 and shown in Figure 4 together with the record of air temperature at AWS4. Periods of high temperatures (T1) often occur in correspondence to downvalley winds (W1) (Figure 4). In colder days, the wind

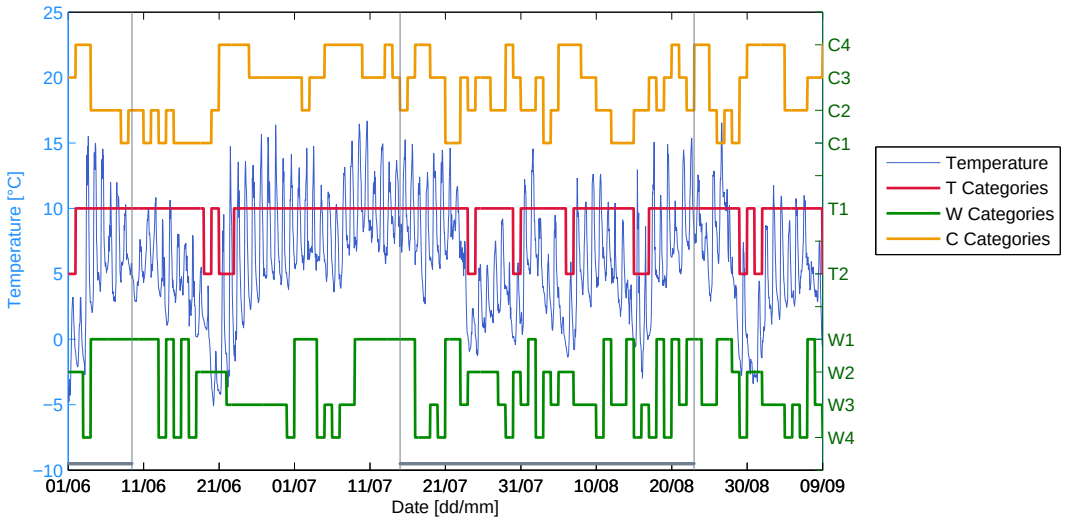

Fig. 4. Time series showing the defined conditions for cloud cover (C1 cloudy, C2 mainly cloudy, C3 partly cloudy, C4 clear-sky), temperature (T1 warm, T2 cold) and wind conditions (W1 downvalley, W2 diurnal switch downvalley/upvalley, W3 variable wind conditions, W4 upvalley) on a daily scale together with observed temperature at AWS4. The common period of observations used in the analysis is indicated by the grey bars at the bottom of the figure.

does not show a clear pattern but a tendency towards upvalley winds. From the temperature record, two main patterns can be observed: a first period of high temperatures (from about 21st of June to 21st of July) and a second period of colder temperature characterised by lower mean values and higher variability (from 21st of July onwards). The stable, warm period (21st of June to 21st of July) is also associated with more stable conditions for wind and cloud cover, with mostly clear sky days (C3 and C4) and wind conditions W1, W2 and W3 (i.e. no upvalley wind).

Assumption of a constant H over the glacier seems a limitation of the model, given that we expect the KBL to be better developed in the lower sections of the glacier. We therefore tested a model version with a variable H along the glacier flowline (GBvarH). Figure 5 shows the model results for the categories listed above for the unmodified model (GB98) described in section 4 and for the modified model (GBvarH), together with the actual temperature measurements. The values of H in correspondence of each T-Logger were found by minimizing the RMSE at each T-Logger for the time series of the common period of record. This corresponds to applying a piece-wise constant H for the different sections of the glacier, as a continuous variability of H would require knowledge of the functional dependency of H with x and the integration of the corresponding equation. Such functional dependency however cannot be inferred from the available data. The configuration resulting from the piece-wise calibration is H =[10 m (TL2, TL3), 14 m (TL7), 16 m (TL8) and 26 m (TL9)].

A number of results are apparent from Figure 5. In most cases the application of a variable boundary layer thickness (GBvarH) is better able to represent the shape of the temperature profile along the flowline than the model assuming a constant boundary layer thickness. Under overcast conditions (C1), the model does not work well with a constant (GB98) nor

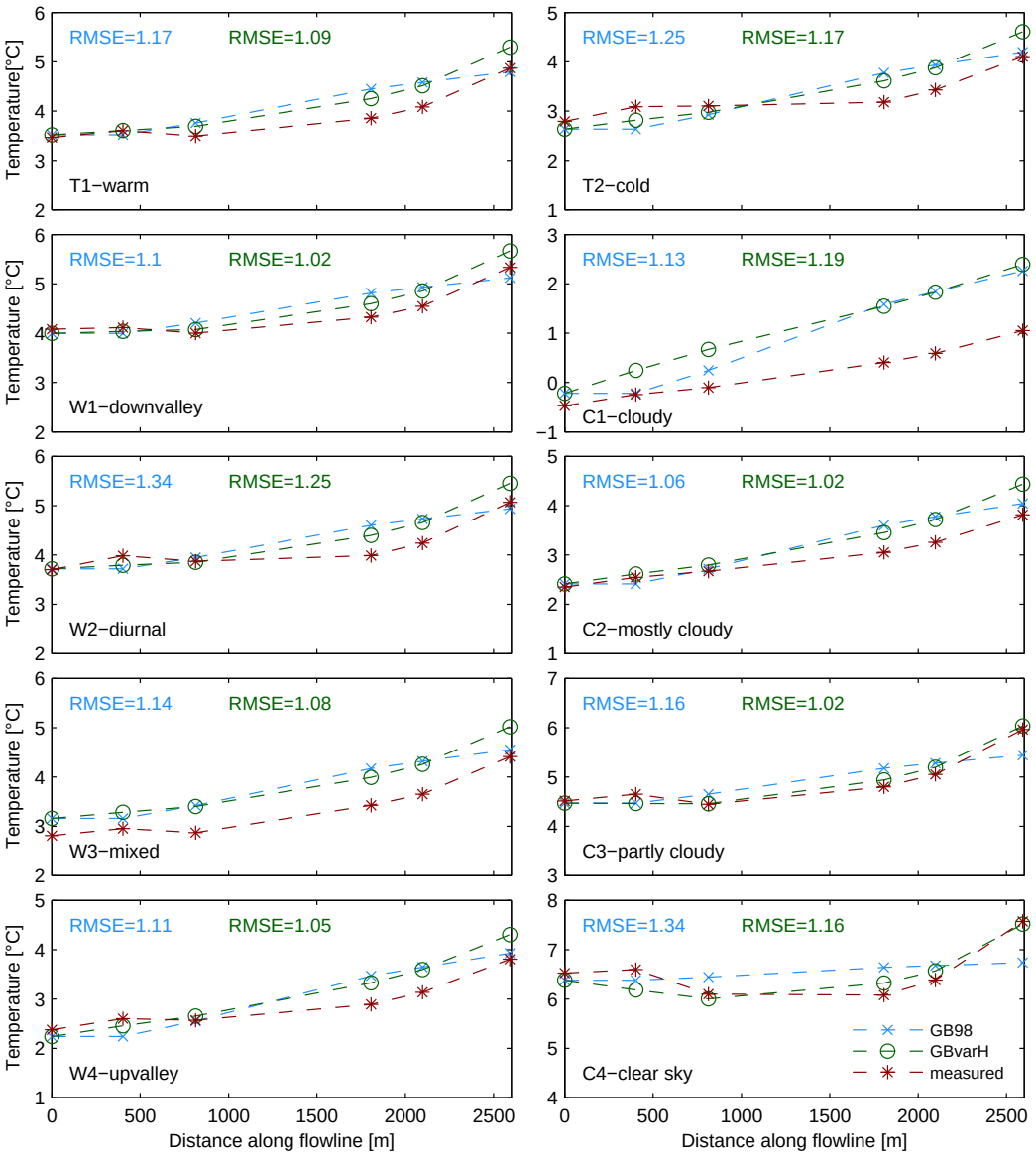

Fig. 5. Measured air temperature along the flowline in comparison with results of the unmodified model (GB98) and model with variable H (GBvarH) for the different climatic conditions described in Table 2.

Table 2. Summary of the climatic categories identified for analysis of the model results, description of criteria and the number of days corresponding to each category

ID	Explanation	Nr. of days whole time series	Nr of days period of common data
T1	80% of hourly temperature data are above 0°C	87	40
T2	all remaining days (cold days)	22	17
W1	at least 80% of hourly wind data in downvalley direction	37	17
W2	at least 60% of hourly wind data in the afternoon (13:00-20:00) in upvalley direction		
	at least 60% of hourly wind data during the rest of the day in downvalley direction	29	10
W3	all days with no clear wind pattern identifiable	25	15
W4	at least 80% of hourly wind measurements in upvalley direction	18	11
C1	cloudy	18	8
C2	mostly cloudy	32	19
C3	partly cloudy	32	16
C4	clear sky	27	10

with a variable H (GBvarH). To support the visual evaluation of model performance (Figure 5), we calculated the RMSE at each T-Loggers and the mean RMSE at all sites to quantitatively assess the model performance for the different conditions. For all conditions, the application of a variable H reduces the RMSE, except for cloudy conditions (cloud category C1) (Figure 5), even though improvements are minor for some of the categories. Both model versions are able to represent the almost linear shape of temperature that corresponds to very cold (cloudy) conditions, but neither can reproduce the correct slope. For all conditions except cloudy days the model performance is highest at TL7 and TL8 (followed by TL9 and then TL2), indicating that the model works best on the lower glacier section under conditions favourable to the development of katabatic wind. The improvement allowed by varying H is stronger on the lower section of the glacier under clear-sky conditions (with a mean improvement in RMSE of 12% in the upper part and of 17% in the lower), as well as under warm temperatures and downvalley winds.

For downvalley wind conditions (W1) and warm temperatures (T1) the fit for the mean values is good. This is evident also from analysis of the mean diurnal cycles at different locations (Figure 6). It is clear that for all conditions except for C1 (overcast days) the agreement between model simulations (with both options) and observations is better at the T-Logger on the tongue (TL8, with a $RMSE = 1.03$ and $RMSE = 1.05$ for all conditions for GBvarH and GB98, respectively) than at

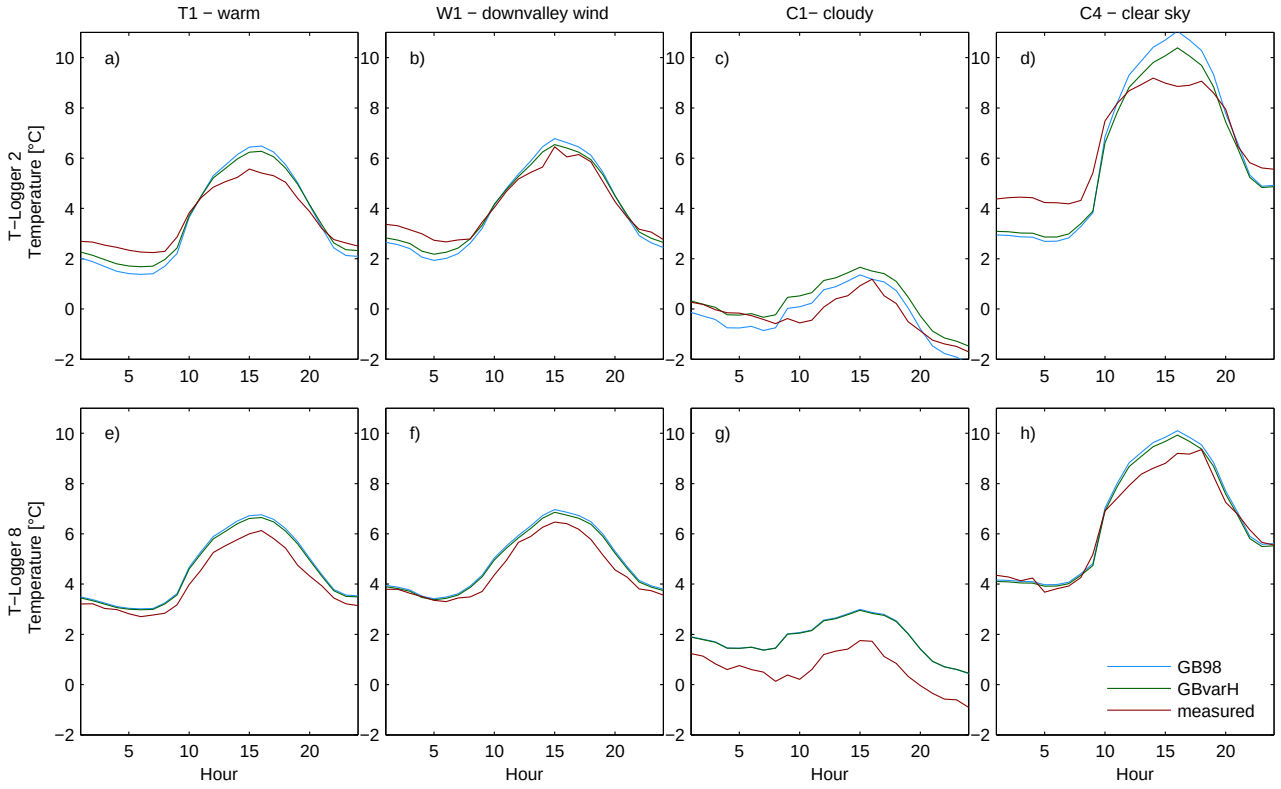

Fig. 6. Mean diurnal cycle of measured air temperature compared with the results of the unmodified model (GB98) and model with variable H (GBvarH) for selected climatic conditions (described in Table 2) at TL2 in the upper section and TL8 in the lower section of the glacier.

the one in the upper section of the glacier (TL2, with a $RMSE = 1.09$ and $RMSE = 1.21$ for all conditions for GBvarH and GB98, respectively). This is mainly due to the underestimation of temperature in the early morning and late evening by the model compared to the observation at TL2 (Figure 6a, b and d), while this effect is no longer visible at TL8 (Figure 6e, f and h). It is also evident that while no difference in model performance can be observed between the two model versions at TL2, the model with variable H (GBvarH) works slightly better at the lower T-Logger. Under cloudy, cold conditions, the fit between modelled and observed average temperatures is poorer for both models especially at TL8 (Figure 6c and g).

6. DISCUSSION AND CONCLUSIONS

The along-glacier temperature distribution at HGdA is poorly represented by a constant linear LR. On the upper glacier, above about 2900 m a.s.l., the LR is typically weak and often positive, indicating a shallow boundary layer and strong temperature stratification in the lowest few m of the atmosphere. Below 2900 m a.s.l. on the glacier tongue, LRs are highly variable but frequently strongly negative particularly when katabatic winds develop. Averaged over the entire glacier over the period of measurement the mean LR is shallower than the ELR. Use of a constant LR calibrated with local data improves the fit to

observed temperature and results in a reduced RMSE. It should be kept in mind, however, that a large amount of data was used to derive the CLRcal and these might not be commonly available. The two methods tested as alternative to a constant LR, GB98 and GBvarH, reduce the RMSE further. The GB98 model in its unmodified form over- or underestimates temperature at most locations and conditions, whereas the GBvarH better captures the shape of the temperature profile along the flowline for most of the weather cases considered, even though an overestimation is still evident. Hence, the assumption of a constant thickness of the glacier boundary layer does not seem to hold for HGdA. The variability in H was also stated by various authors and partly ascribed to the larger fetch for katabatic winds towards the tongue of the glacier (e.g. Strasser and others, 2004; Shea and Moore, 2010). The correspondence of mainly downvalley winds (W1) with high temperature agrees with the general prerequisite of a high temperature deficit favoring the development of katabatic wind (e.g. Ohata, 1989; Greuell and others, 1997; Klok and others, 2005; Pellicciotti and others, 2008; Shea and Moore, 2010). Under such conditions the GB98 model would be expected to work best, as the main requirements, the presence of a glacier wind and temperatures higher than 0°C, are fulfilled (see Greuell and Böhm, 1998). For clear sky days (C4), as well as partly cloudy days (C3), the better performance of GBvarH on the lower part of the glacier corresponds with the better development of katabatic winds further down on the glacier due to topographic constraints (e.g. Strasser and others, 2004; Shea and Moore, 2010), such as the narrowing towards the tongue. High radiation on sunny and clear sky days (C3 and C4) produces warm ambient air that is cooled by the ice surface (Stenning and others, 1981), and the strong adiabatic warming on the lower part of the tongue is well captured by the GBvarH model. In contrast, the poor performance on cloudy days (C1), when temperatures are overestimated for most of the glacier, might be due to the fact that the solar warming process is reduced by the presence of clouds, and the lower temperature deficit prevents the development of katabatic flows, a prerequisite of the model (Greuell and Böhm, 1998). A possible reason for the poor performance of GB98, especially on the tongue, might be local effects. The influence of warming from surrounding slopes and debris patches could be an additional explanation for the steep increase in temperature at TL9, but it is impossible to test such hypotheses without more data. It is also difficult to envisage the processes whereby warm air over the moraines can be transferred to the T-Logger stations, as heat advection would require cross-glacier wind which does not seem to occur on the tongue. The other process that could be responsible for such warming is longwave radiation emission. At the glacier tongue the valley narrows to about 500 m width so that emission from the snow-free slopes might be more important than in the upper section. This effect, however, is difficult to quantify and seems to be small according to a study by Juszak and Pellicciotti (2012). It is difficult to identify the main reasons for the observed temperature variability with the limited amount of data available and our study clearly points to the need to improve our understanding of temperature variability over glaciers. For a quantification of these local effects the number of measurement sites should be expanded.

The conclusion that GBvarH works better than the original model means that we need a variable L_R (length scale) in the model which can be due to an actual variability in H along the glacier flowline or to a variable c_H. The validity of the assumption that c_H is constant should be investigated by full energy balance calculations, while more knowledge should be gained on the actual height of the GBL as well as its variability in space and main controls.

Some studies have found katabatic wind acceleration at night following radiative cooling (Manins and Sawford, 1979; Horst and Doran, 1986). The model is able to capture this possible behavior in the lower part of the glacier, but underestimates temperature in the upper part (see Figure 6). This again suggests a strong temperature stratification in the lowest few m of the atmosphere in the upper part of the glacier, where the boundary atmospheric layer is poorly developed due to a short fetch. Under such conditions, the 2 m measurement height is likely to be outside of the 'constant flux layer' where the atmosphere is fully adjusted to the underlying surface, and a basic assumption of most energy-balance melt models will not be met in any case. As above, only more data on the height and characteristics of the GBL can provide a clear explanation for the observed variability at night.

The main conclusions of this study are that:

The GB98 model is an improvement over the assumption of a constant LR, even when locally calibrated, as demonstrated by a reduction in the RMSE.

For HGdA, the model works better when different glacier boundary layer thicknesses, H, are used for different sections of the glacier, as it captures the shape of the along-glacier temperature distribution and replicates the actual temperatures better.

The model works better for clear sky conditions and high temperatures as the greater temperature deficit typical of these cases favors the development of a katabatic wind, which commonly occurs under sunny summer conditions.

The model does not work well for cloudy conditions.

It is also apparent from our results that no readily applicable model exists to derive distributed temperature field over a glacier, nor any can be developed without additional measurements sheading light on the height and characteristics of the KBL.

Overall, the performance of GB98 is found to be acceptable under conditions and locations where a katabatic wind can develop, and represents an improvement over the use of a constant LR. However, different models for air temperature distribution are needed: in areas where the fetch is short or gradients are shallow; under cool and/or cloudy conditions; and when synoptic

forcing of the wind dominates. Our results provide evidence for a possible variability of the height of the GBL that should be supported by experimental evidence. Our measurements are inadequate to investigate the height and structure of the GBL, which would require tower measurements at different heights. Our results, however, seem to clearly call for an increase of such experiments and should give inputs for this sort of investigation. The finding that better results can be obtained by allowing the height of the GBL to vary long the glacier flowline should be tested for other sites.

In this work we compared four options for modelling air temperature with respect to their ability to reproduce the observed temperatures. Differences are evident but are in some cases small. The effect that each method would have on the magnitude of simulated melt and mass balance should also be evaluated.

GB98 and GBvarH can partly explain the low sensitivity of GBL temperature to external atmospheric temperature changes, and so help address an important challenge in estimating glacier response to climatic changes. Successful application of the model requires knowledge of the initiation point for katabatic flows, however, and this would probably require local calibration data in most cases. Supported by new field data, future research should focus on incorporating different physical conditions and topographic effects in order to develop a model able to reproduce realistic temperature data time-series throughout the glacier which would be a milestone achievement for melt modelling in general.

7. ACKNOWLEDGEMENTS

The authors would like to thank all the people involved in the field campaign 2010: Andreas Bauder, Cyrill Buergi, Ilaria Clemenzi, Jacopo Sanfilippo, Jakob Helbing, Lea Mueller, Luca Salvatore, Luzia Sturzenegger, Markus Konz, Martin Heynen, Maurizio Savina, Mauro Bruno, Roger Bordoy Molina, Tim Reid. Thomy Keller helped us build the structure for the T-Loggers. The authors are grateful to Prof. Paolo Burlando for supporting MC and the field campaign on HGdA.

References

Arnold, N. S., W. G.Rees, A. J. Hodson and J. Kohler, 2006. Topographic controls on the surface energy balance of a high Arctic valley glacier, *Journal of Geophysical Research*, **111**(F2), F02011.

Arnold, N. S., I. C. Willis, M. J. Sharp, K. S. Richards and W. J. Lawson, 1996. A distributed surface energy–balance model for a small valley glacier. I. Development and testing for Haut Glacier d'Arolla, Valais, Switzerland, *Journal of Glaciology*, **42**(140), 77–89.

Braithwaite, R. J., Y. Zhang and S. C. B. Raper, 2002. Temperature sensitivity of the mass balance of mountain glaciers and ice caps as a climatological characteristic, *Zeitschrift für Gletscherkunde und Glazialgeologie*, **1**, 35–61.

Brock, B., C. Mihalcea, M. Kirkbride, G. Diolaiuti, M. Cutler and C. Smiraglia, 2010. Meteorology and surface energy fluxes in 2005-2007 ablation seasons at Miage debris-covered glacier, Mont Blanc Massif, Italian Alps, *Journal of Geophysical*

Research, **115**(D9), D09106.

Brock, B. W. and N. S. Arnold, 2000. A spreadsheet-based (Microsoft Excel) point surface energy balance model for glacier and snow melt studies, *Earth Surface Processes and Landforms*, **25**(6), 649–658.

Brock, B. W., I. C. Willis and M. J. Sharp, 2006. Measurement and parameterization of aerodynamic roughness length variations at Haut Glacier d'Arolla, Switzerland, *Journal of Glaciology*, **52**(177), 281–297.

Brutsaert, W., 1975. On a derivable formula for long-wave radiation from clear skies, *Water Resources Research*, **11**(5), 742–744.

Carenzo, M., F. Pellicciotti, S. Rimkus and P. Burlando, 2009. Assessing the transferability and robustness of an enhanced temperature-index glacier-melt model, *Journal of Glaciology*, **55**(190), 258–274.

Chutko, K. J. and S. F. Lamoureux, 2009. The influence of low-level thermal inversions on estimated melt-season characteristics in the central Canadien Arctic, *International Journal of Climatology*, **29**(2), 259–268.

Farinotti, D., S. Usselmann, M. Huss, A. Bauder and M. Funk, 2012. Runoff evolution in the Swiss Alps: projections for selected high-alpine catchments based on ENSEMBLES scenarios, *Hydrological Processes*, **26**(13), 1909–1924.

Gardner, A. S. and M. Sharp, 2009. Sensitivity of net mass-balance estimates to near-surface temperature lapse rates when employing the degree-day method to estimate glacier melt, *Annals of Glaciology*, **50**(50), 80–86.

Gardner, A. S., M. J. Sharp, R. M. Koerner, C. Labine, S. Boon, S. J. Marshall, D. O. Burgess and D. Lewis, 2009. Near-Surface Temperature Lapse Rates over Arctic Glaciers and Their Implications for Temperature Downscaling, *Journal of Climate*, **22**(16), 4281–4298.

Greuell, W and R. Böhm, 1998. 2 m temperatures along melting mid-latitude glaciers, and implications for the sensitivity of the mass balance to variations in temperature, *Journal of Glaciology*, **44**(146), 9–20.

Greuell, W., W. H. Knap and P. C. Smeets, 1997. Elevational changes in meteorological variables along a midlatitude glacier during summer, *Journal of Geophysical Research*, **102**(D22), 25941–25954.

Hock, R. and B. Holmgren, 2005. A distributed surface energy-balance model for complex topography and its application to Storglaciären, Sweden, *Journal of Glaciology*, **51**(172), 25–36.

Horst, T. W. and J. C. Doran, 1986. Nocturnal drainage flow on simple slopes, *Boundary-Layer Meteorology*, **34**(3), 263–286.

Hulth, J., C. Rolstad, K. Trondsen and R. Wedøe Rødby, 2010. Surface mass and energy balance of Sørbreen, Jan Meyen, 2008, *Annals of Glaciology*, **51**(55), 110–119.

Huss, M., A. Bauder, M. Funk and R. Hock, 2008. Determination of the seasonal mass balance of four Alpine glaciers since 1865, *Journal of Geophysical Research*, **113**(F1), F01015.

Juszak, I. and F. Pellicciotti, 2012. A comparison of parameterisations of incoming longwave radiation over melting glaciers: model robustness and seasonal variability, in revision (JGR).

Klok, E. J., M. Nolan and M. R. Van den Broeke, 2005. Analysis of meteorological data and the surface energy balance of McCall Glacier, Alaska, USA, *Journal of Glaciology*, **51**(174), 451–461.

Klok, E. J. and J. Oerlemans, 2002. Model study of the spatial distribution of the energy and mass balance of Morteratschgletscher, Switzerland, *Journal of Glaciology*, **48**(163), 505–518.

Li, X. and M. W. Williams, 2008. Snowmelt runoff modelling in an arid mountain watershed, Tarim Basin, China, *Hydrological Processes*, **22**(19), 3931–3940, doi:10.1002/hyp.7098.

Machguth, H., F. Paul, M. Hoelzle and W. Haeberli, 2006. Distributed glacier mass-balance modelling as an important component of modern multi-level glacier monitoring, *Annals of Glaciology*, **43**(1), 335–343.

Manins, P. C. and B. L. Sawford, 1979. A model of katabatic wind, *Journal of Atmospheric Science*, **36**(4), 619–630.

Marshall, S. J. and M. J. Sharp, 2008. Temperature and Melt Modeling on the Prince of Wales Ice Field, Canadian High Arctic, *Journal of Climate*, **22**, 1454–1468.

Marshall, S. J., M. J. Sharp, D. O. Burgess and F. S. Anslow, 2007. Near-surface-temperature lapse rates on the Prince of Wales Icefield, Ellesmere Island, Canada: implications for regional downscaling of temperature, *International Journal of Climatology*, **27**(3), 385–398.

Marty, C. and R. Philipona, 2000. The clear-sky index to separate clear-sky from cloudy-sky situations in climate research, *Geophysical Research Letters*, **27**(17), 2649–2652.

Michlmayr, G., M. Lehning, G. Koboltschnig, H. Holzmann, M. Zappa, R. Mott and W. Schner, 2008. Application of the Alpine 3D model for glacier mass balance and glacier runoff studies at Goldbergkees, Austria, *Hydrological Processes*, **22**(19), 3941–3949, doi: 10.1002/hyp.7102.

Minder, J. R., P. W. Mote and J. D. Lundquist, 2010. Surface temperature lapse rates over complex terrain: Lessons from the Cascade Mountains, *Journal of Geophysical Research*, **115**(D14), D14122.

Nienow, P., M. Sharp and I. Willis, 1996. Temporal Switching between Englacial and Subglacial Drainage Pathways: Dye Tracer Evidence from the Haut Glacier d'Arolla, Switzerland, *Geografiska Annaler. Series A, Physical Geography*, **78**(1), 51–60.

Nolin, A. W., J. Phillippe, A. Jefferson and S. L. Lewis, 2010. Present-day and future contributions of glacier runoff to summertime flows in a Pacific Northwest watershed: Implications for water resources, *Water Resources Research*, **46**(W12), W12509.

399 Ohata, T., 1989. Katabatic wind on melting snow and ice surfaces (I.) Stationary wind on a large maritime glacier, *Journal*
400 *of the Meteorological Society of Japan*, **67**, 99–112.
401 Paul, F., H. Escher-Vetter and H. Machguth, 2009. Comparison of mass balances for Vernagtferner, Oetzal Alps, as obtained
402 from direct measurements and distributed modeling, *Annals of Glaciology*, **50**(50), 169–177.
403 Pellicciotti, F., B. Brock, U. Strasser, P. Burlando, M. Funk and J. Corripio, 2005. An enhanced temperature-index glacier
404 melt model including the shortwave radiation balance: development and testing for Haut Glacier d'Arolla, Switzerland,
405 *Journal of Glaciology*, **51**(175), 573–587.
406 Pellicciotti, F., J. Helbing, A. Rivera, V. Favier, J. Corripio, J. Araos, J.-E. Sicart and M. Carenzo, 2008. A study of the
407 energy balance and melt regime on Juncal Norte Glacier, semi-arid Andes of central Chile, using melt models of different
408 complexity, *Hydrological Processes*, **22**(19), 3980–3997.
409 Pepin, N. and M. Losleben, 2002. Climate change in the Colorado Rocky Mountains: Free air versus surface temperature
410 trends, *International Journal of Climatology*, **22**(3), 311–329.
411 Petersen, L. and F. Pellicciotti, 2011. Spatial and temporal variability of air temperature on a melting glacier: Atmospheric
412 controls, extrapolation methods and their effect on melt modeling, Juncal Norte Glacier, Chile, *Journal of Geophysical*
413 *Research*, **116**(D23), D23109.
414 Shea, J. M. and R. D. Moore, 2010. Prediction of spatially distributed regional-scale fields of air temperature and vapor
415 pressure over mountain glaciers, *Journal of Geophysical Research*, **115**(D23), D23107.
416 Stahl, J., R. D. Moore, J. A. Floyer, M.G. Asplin and I.G. McKendry, 2006. Comparison of approaches for spatial interpolation
417 of daily air temperature in a large region with complex topography and highly variable station density, *Agricultural and*
418 *Forest Meteorology*, **139**(3–4), 224–236.
419 Stenning, A. J., C. E. Banfield and G. J. Young, 1981. Synoptic controls over katabatic layer characteristics above a melting
420 glacier, *International Journal of Climatology*, **1**(4), 309–324.
421 Strasser, U., J. Corripio, F. Pellicciotti, P. Burlando, B. Brock and M. Funk, 2004. Spatial and temporal variability of meteo-
422 rological variables at Haut Glacier d'Arolla (Switzerland) during the ablation season 2001: Measurements and simulations,
423 *Journal of Geophysical Research*, **109**(D3), D03103.
424 Stull, R.B., 1988. An introduction to boundary layer meteorology, Springer.
425 van den Broeke, M. R., 1997. Structure and diurnal variation of the atmospheric boundary layer over a mid–latitude glacier
426 in summer, *Boundary-Layer Meteorology*, **83**(2), 183–205.
427 Willis, I., N. Arnold and B. Brock, 2002. Effect of snowpack removal on energy balance, melt and runoff in a small supraglacial
428 catchment, *Hydrological Processes*, **16**(14), 2721–2749.